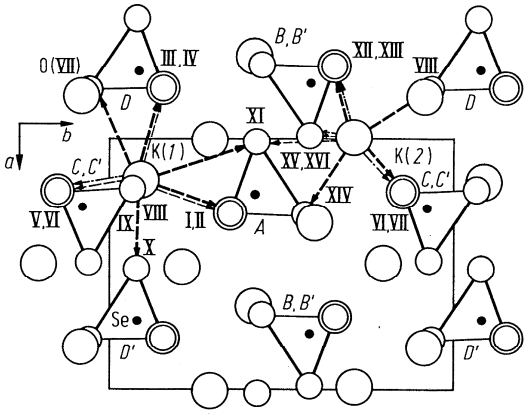

Fig. 39A-2-001. K_2SeO_4. Structure of phase II [70Kal]. Projection on (001). Potassium atoms are shown by large circles, oxygen atoms by smaller open circles, and selenium atoms by small full circles. For numbering of atoms, see Table 39A-2-002 and Table 39A-2-005. Tetrahedra are labelled by capital letters. Pairs of dashed lines indicate contacts to a pair of atoms belonging to the same tetrahedron. A dashed line paired with a dash-dot line indicates that the pair of superposed atoms belong to different tetrahedra.

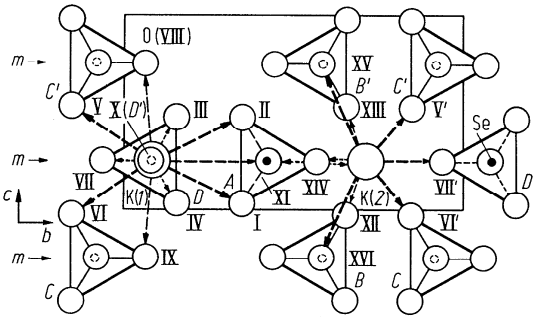

Fig. 39A-2-002. K_2SeO_4. Structure of phase II [70Kal]. Projection on (100). See caption of Fig. 39A-2-001 for symbols and notations. *m*: mirror plane.

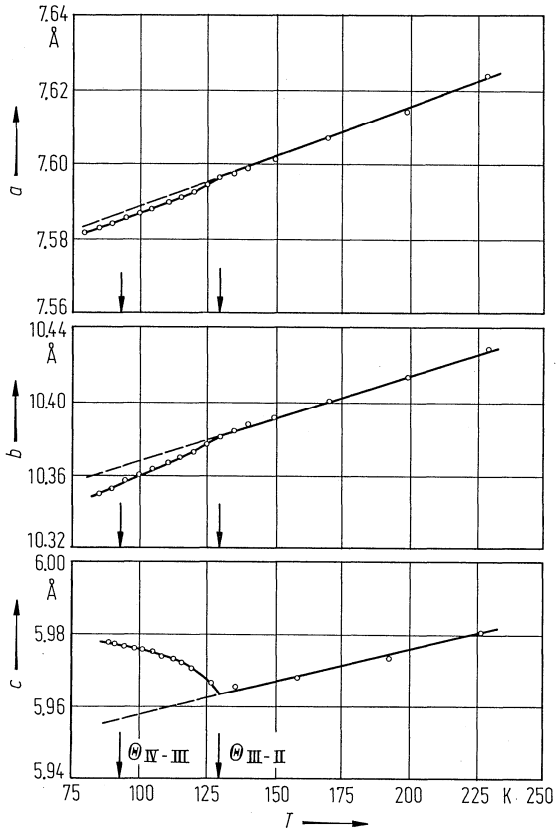

Fig. 39A-2-003. K_2SeO_4. *a*, *b*, *c* vs. *T* [81Kud2]. *a*, *b*, *c*: basic lattice parameters.

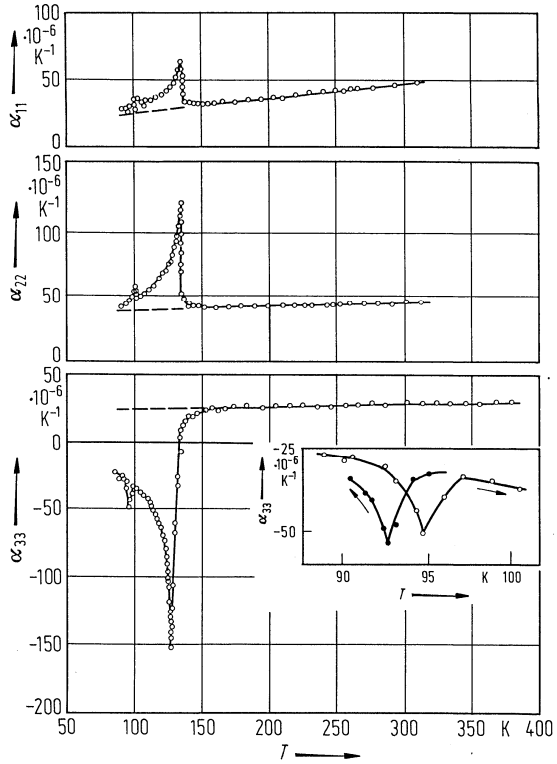

Fig. 39A-2-004. K_2SeO_4. α_{ii} vs. T [82Fle]. α_{11}, α_{22}, α_{33}: linear thermal expansion coefficients along the *a*, *b* and *c* axes.

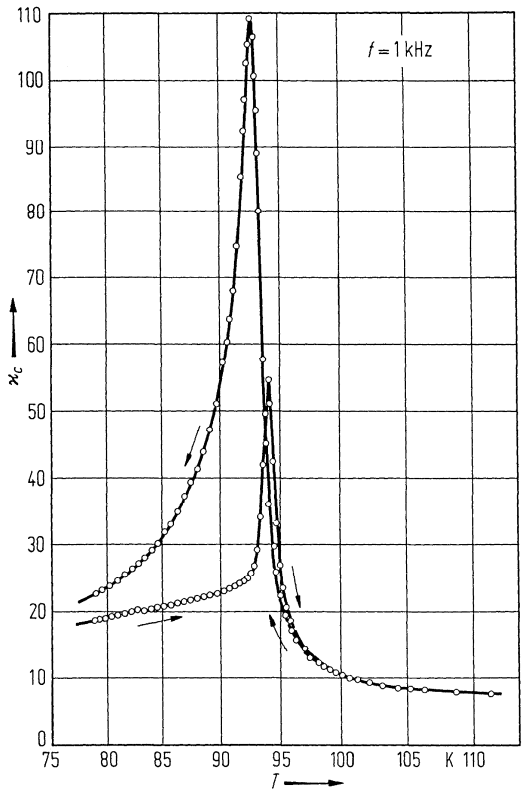

Fig. 39A-2-005. K_2SeO_4. $\varkappa_c$ vs. T [70Aik1].

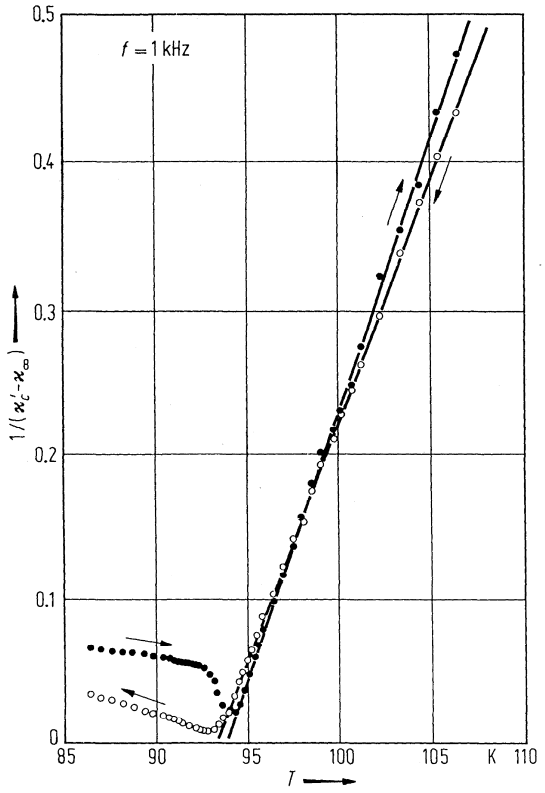

Fig. 39A-2-006. K_2SeO_4. $1/(\kappa_c' - \kappa_\infty)$ vs. T [70Aik1]. $\kappa_\infty = 6.14$.

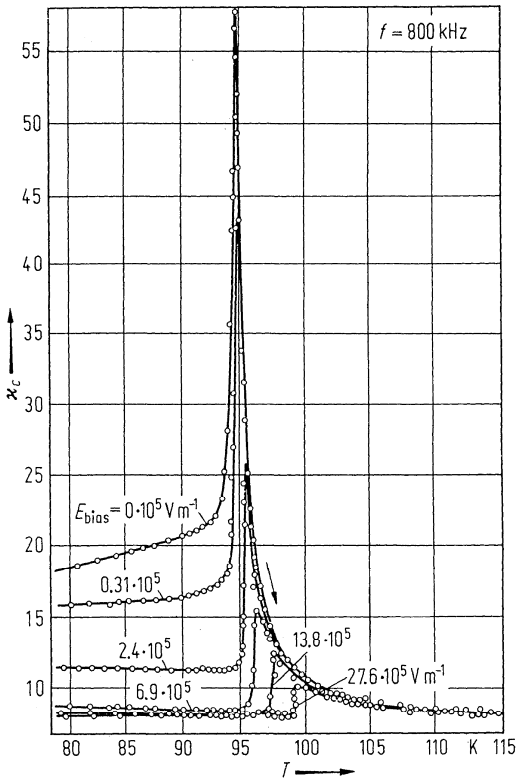

Fig. 39A-2-007. K_2SeO_4. κ_c vs. T [70Aik1]. Parameter: E_{bias}.

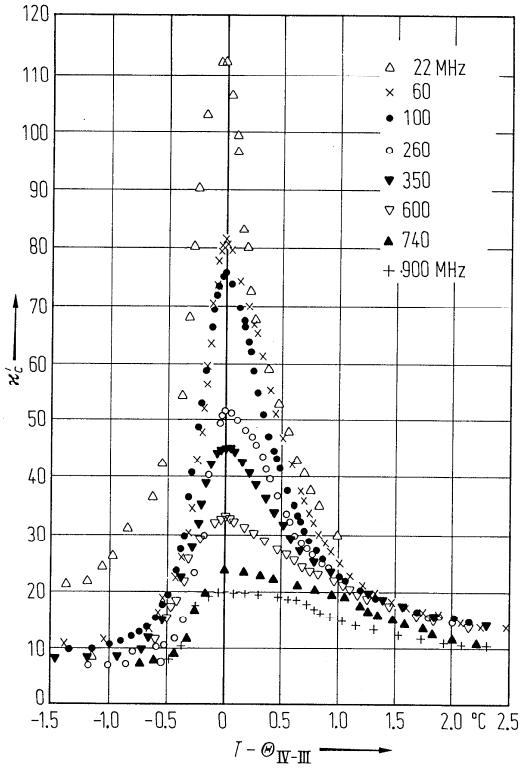

Fig. 39A-2-008. K_2SeO_4. κ_c' vs. $T - \Theta_{IV-III}$ [80Hor]. Parameter: *f*.

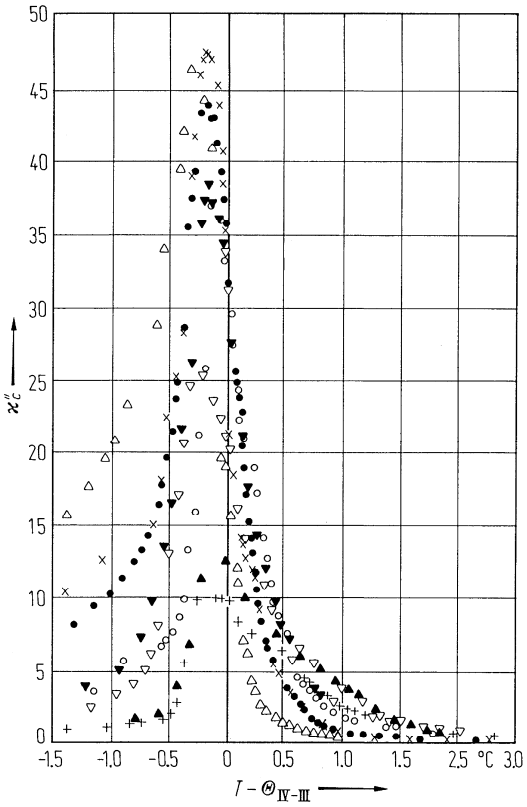

Fig. 39A-2-009. K_2SeO_4. κ_c'' vs. $T - \Theta_{IV-III}$ [80Hor]. For different symbols, see Fig. 39A-2-008.

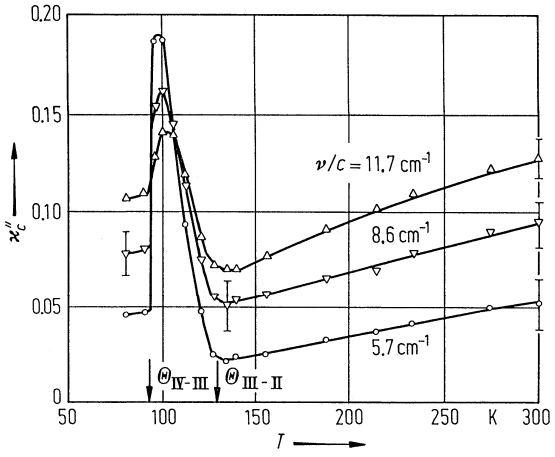

Fig. 39A-2-010. K_2SeO_4. κ_c'' vs. T [80Vol1]. Parameter: ν/c. κ_c'' : imaginary part of the dielectric constant measured by submillimeter waves.

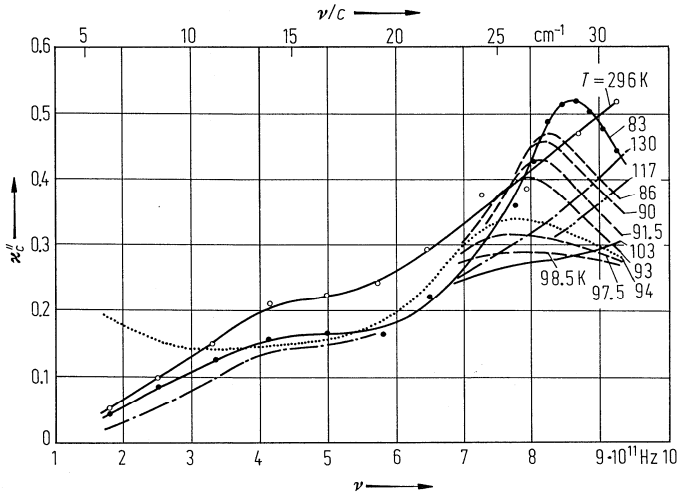

Fig. 39A-2-011. K_2SeO_4. κ_c'' vs. ν [80Vol2]. Parameter: T. κ_c'' : imaginary part of the dielectric constant measured by submillimeter waves.

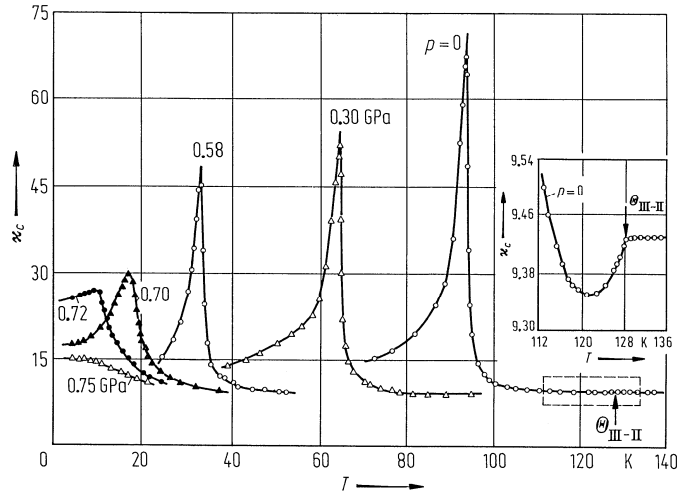

Fig. 39A-2-012. K_2SeO_4. κ_c vs. T [81Sam]. Parameter: p.

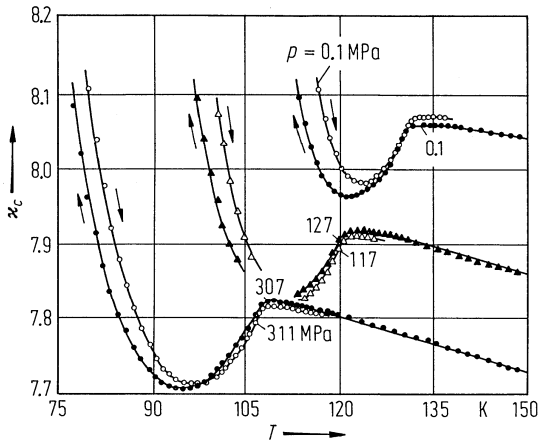

Fig. 39A-2-013. K_2SeO_4. κ_c vs. T in the vicinity of Θ_{III-II} [81Kud1]. Parameter: p. Full circle, full triangle: on cooling, open circle, open triangle: on heating.

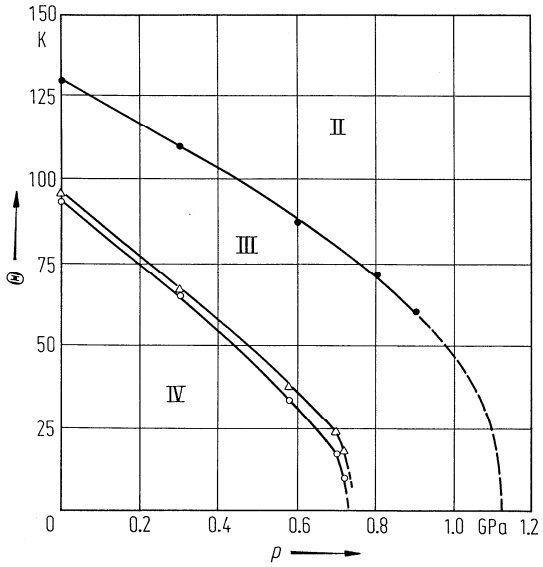

Fig. 39A-2-014. K_2SeO_4. Θ vs. p [81Sam]. Open circle: on cooling, open triangle: on heating.

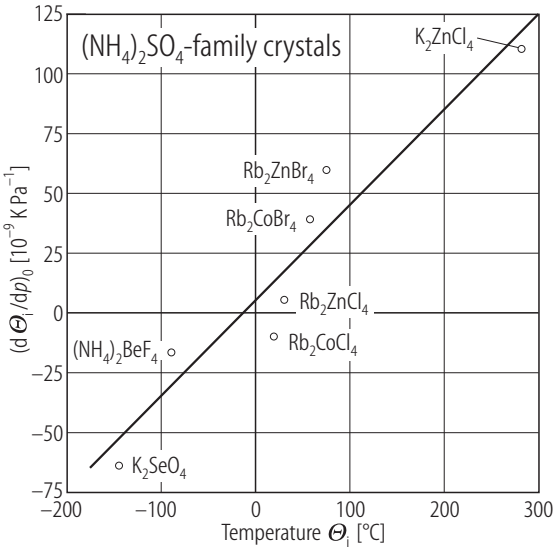

Fig. 39A-2-015. K_2SeO_4, $(NH_4)_2BeF_4$, Rb_2CoCl_4, K_2ZnCl_4, Rb_2ZnCl_4, Rb_2CoBr_4, Rb_2ZnBr_4. $(d\Theta_i/dp)_0$ vs. Θ_i [90Ges]. Θ_i: paraelectric to incommensurate transition temperature. $\Theta_i = \Theta_{III-II}$ for K_2SeO_4, and $\Theta_i = \Theta_{II-I}$ for the other crystals.

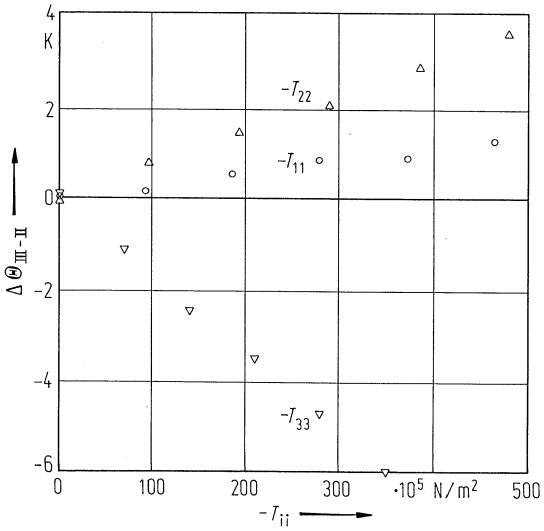

Fig. 39A-2-016. K_2SeO_4. $\Delta\Theta_{III-II}$ vs. $-T_{ii}$ [85Bil]. $\Delta\Theta_{III-II}$: shift of the transition temperature Θ_{III-II}. T_{ii}: uniaxial stress.

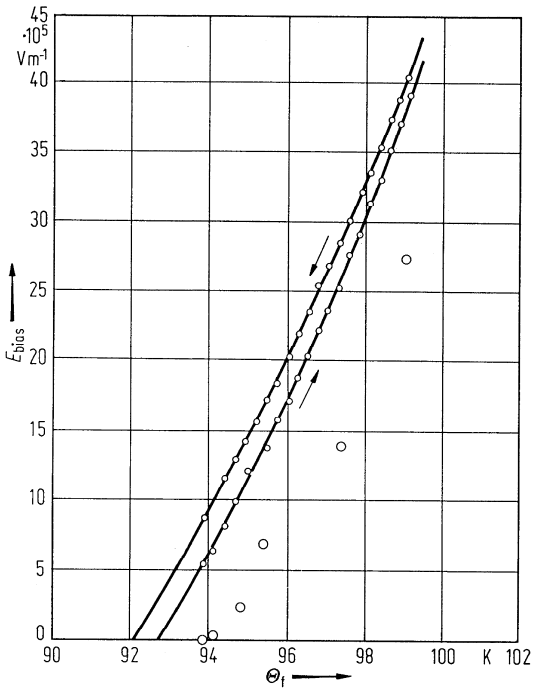

Fig. 39A-2-017. K_2SeO_4. E_{bias} vs. Θ_f [70Aik1]. Small circles are data obtained from double hysteresis loop, and large circles are those from dielectric measurement.

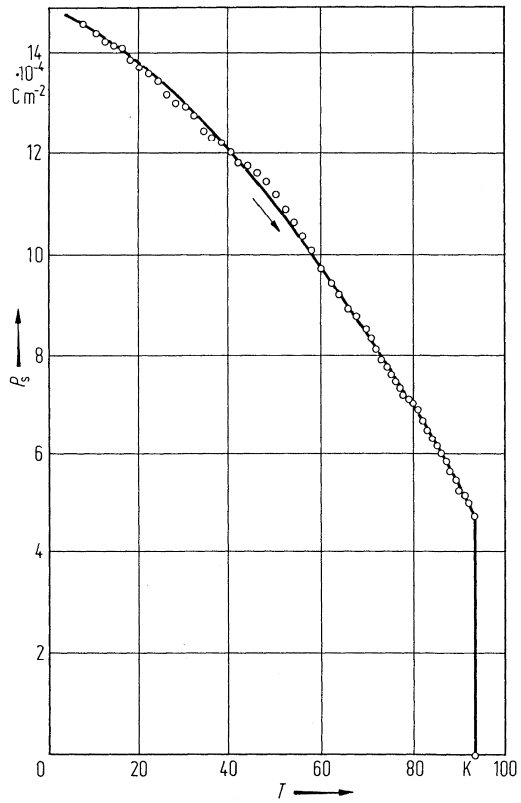

Fig. 39A-2-018. K_2SeO_4. P_s vs. T [70Aik1]. Ferroelectric hysteresis loop measurement. f = 60 Hz.

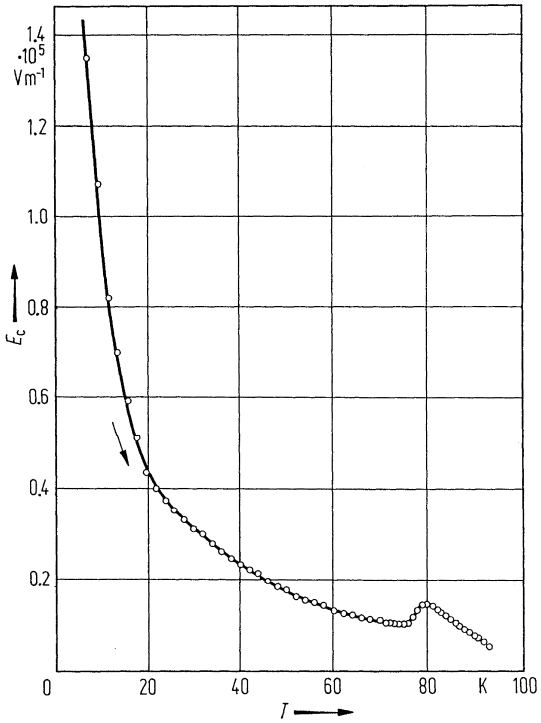

Fig. 39A-2-019. K_2SeO_4. E_c vs. T [70Aik1]. Ferroelectric hysteresis loop measurement. f = 60 Hz.

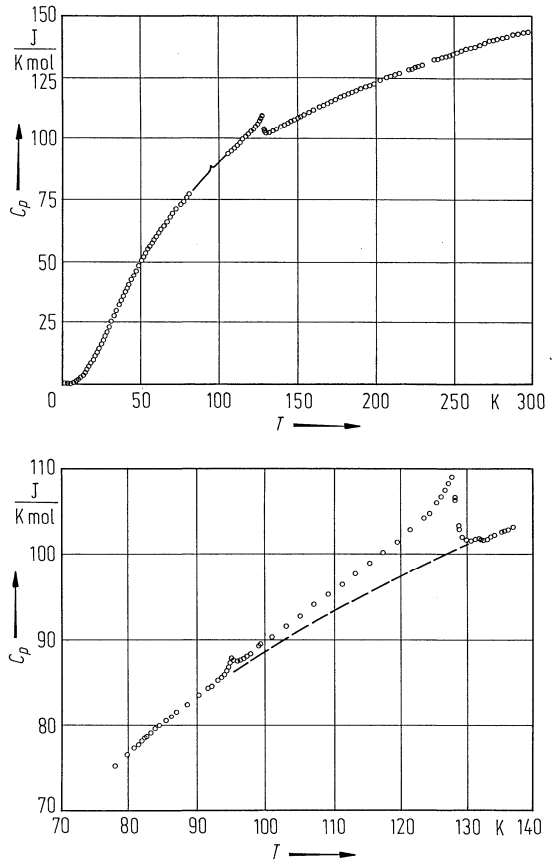

Fig. 39A-2-020. K_2SeO_4. C_p vs. T [81Cha]. C_p: molar heat capacity at constant pressure.

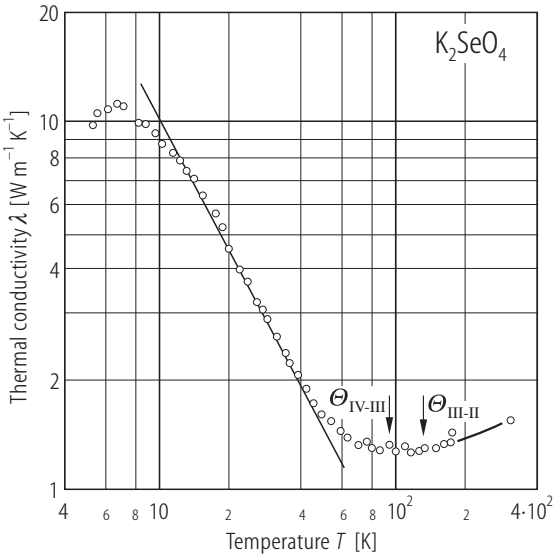

Fig. 39A-2-021. K_2SeO_4. λ vs. T [86Spo]. λ: thermal conductivity along the c axis.

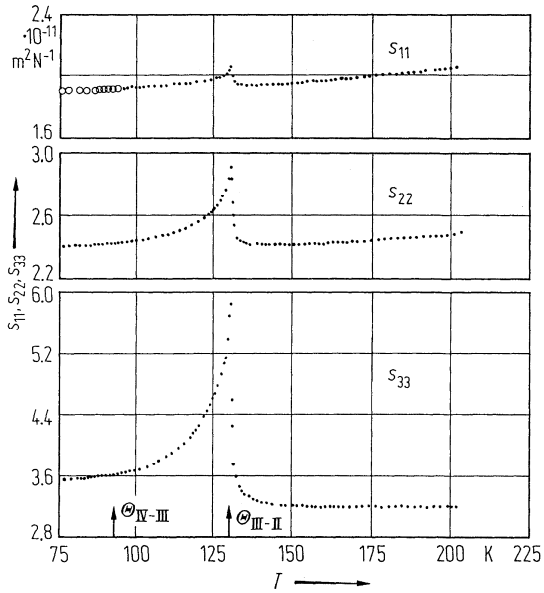

Fig. 39A-2-022. K_2SeO_4. $s_{\lambda\mu}$ vs. T [80Kud]. Composite-bar method.

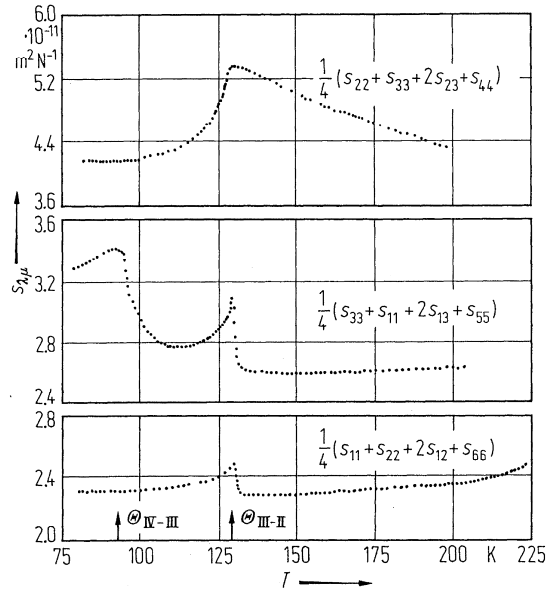

Fig. 39A-2-023. K_2SeO_4. $s_{\lambda\mu}$ vs. T [80Kud]. Composite-bar method.

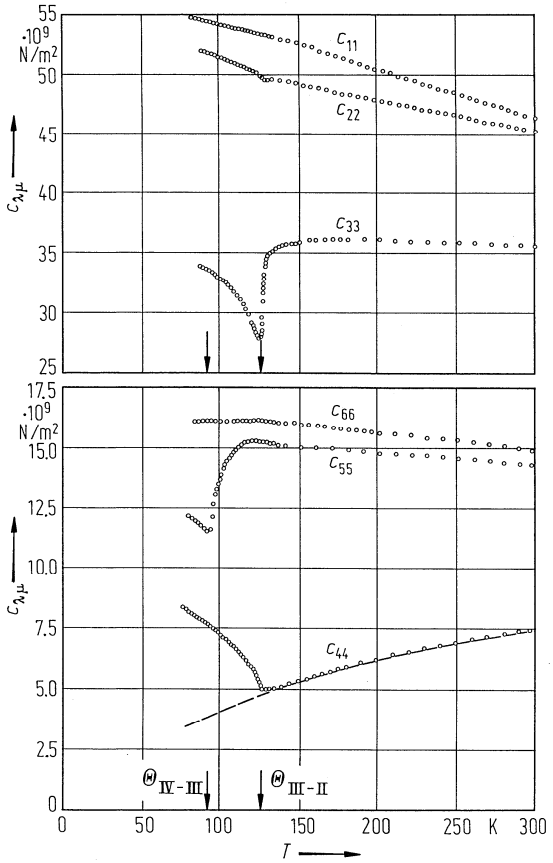

Fig. 39A-2-024. K_2SeO_4. $c_{\lambda\mu}$ vs. T [80Reh]. $c_{\lambda\mu}$: elastic stiffness. f = 15 MHz.

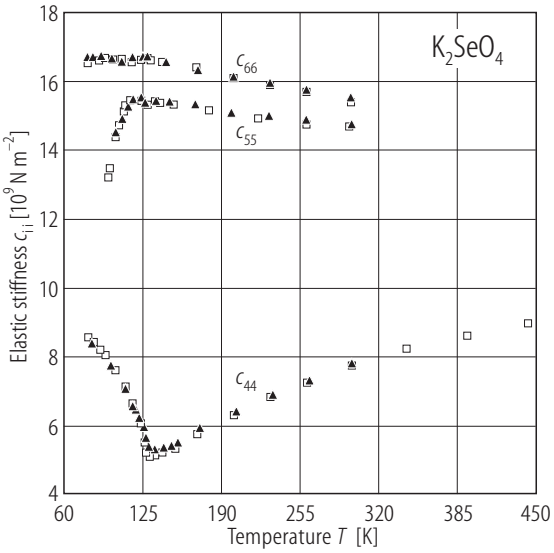

Fig. 39A-2-025. K_2SeO_4. c_{ii} vs. T [91Li]. 90°-Brillouin scattering. λ = 488 nm. c_{44} of squares: $\boldsymbol{q} \parallel b$, $\boldsymbol{u} \parallel c$; triangles: $\boldsymbol{q} \parallel c$, $\boldsymbol{u} \parallel b$. c_{55} of squares: $\boldsymbol{q} \parallel a$, $\boldsymbol{u} \parallel c$; triangles: $\boldsymbol{q} \parallel c$, $\boldsymbol{u} \parallel a$. c_{66} of squares: $\boldsymbol{q} \parallel a$, $\boldsymbol{u} \parallel b$; triangles: $\boldsymbol{q} \parallel b$, $\boldsymbol{u} \parallel a$. $\boldsymbol{q}$: wave number vector, $\boldsymbol{u}$: polarization vector.

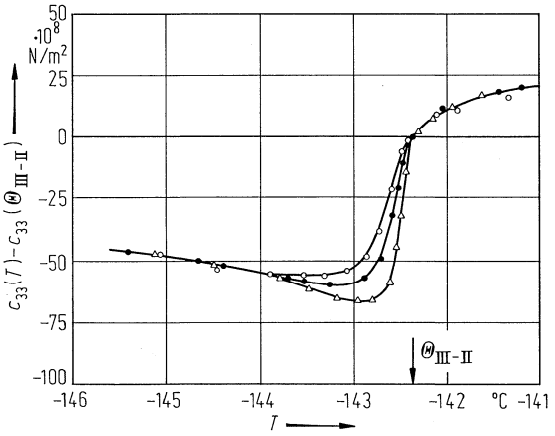

Fig. 39A-2-026. K_2SeO_4. $c_{33}(T) - c_{33}(\Theta_{III-II})$ vs. T [84Lus1]. Parameter: scattering angle ϕ. $c_{33}(\Theta_{III-II})$: elastic stiffness c_{33} at Θ_{III-II}. Brillouin scattering, $\lambda = 514.5$ nm. Open triangle: $\phi = 45°$, full circle: $\phi = 90°$, open circle: $\phi = 135°$.

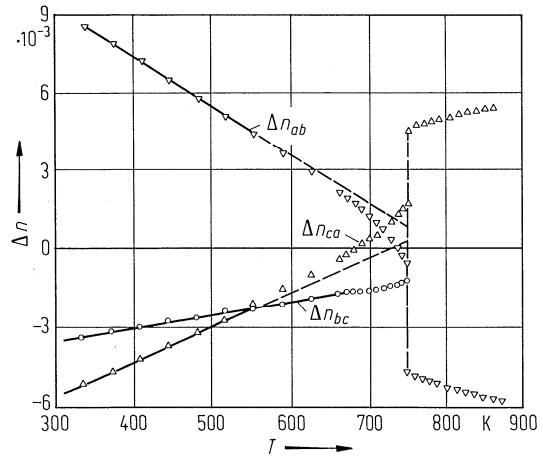

Fig. 39A-2-027. K_2SeO_4. Δn vs. T [81Unr].

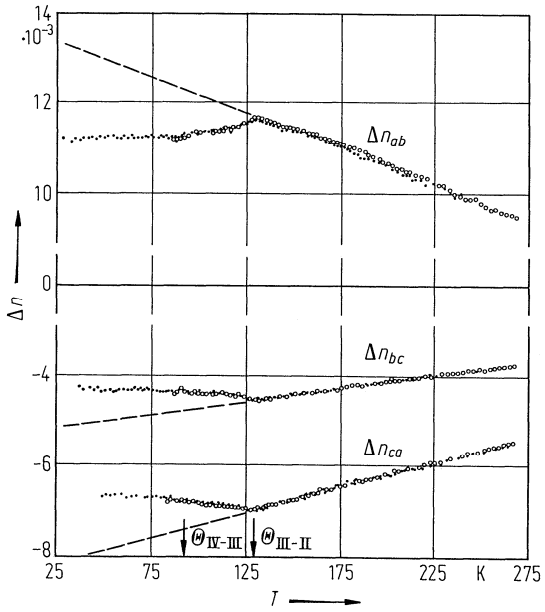

Fig. 39A-2-028. K_2SeO_4. Δn vs. T [81Kud2]. NaD light.

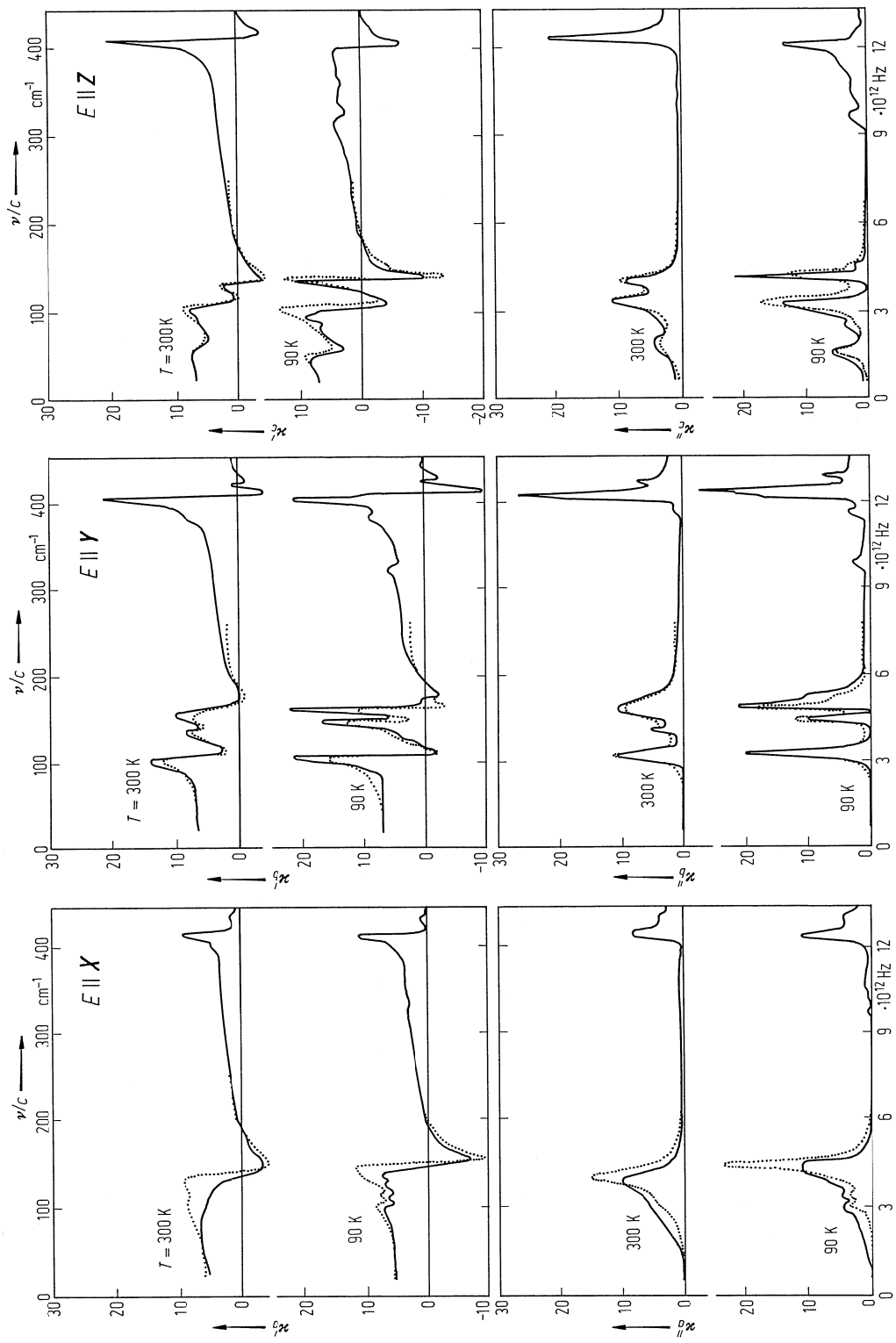

Fig. 39A-2-029. K_2SeO_4. κ', κ'' vs. ν [79Pet]. Parameter: T. The full curves were obtained from reflectivity data using Kramers-Kronig relation. The dotted curves are results of oscillator fit.

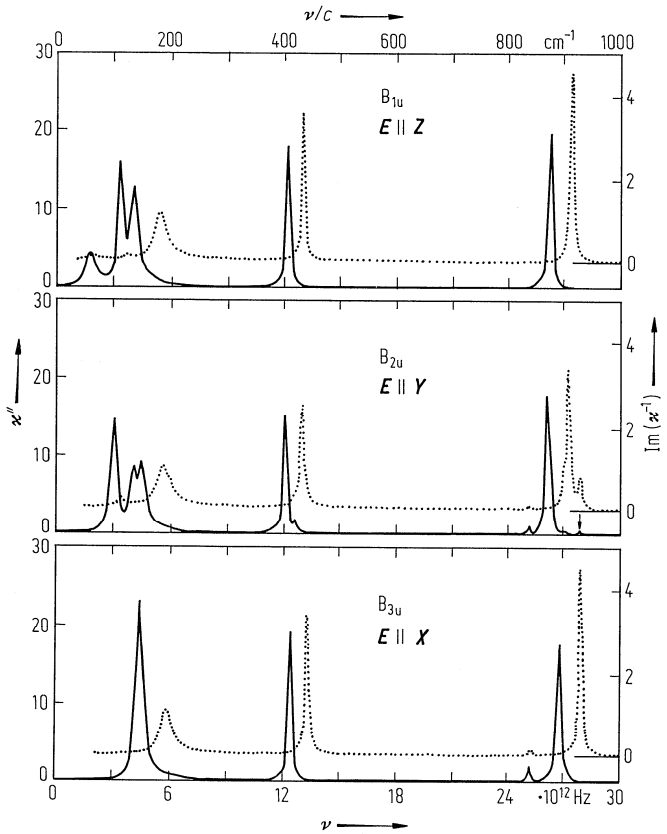

Fig. 39A-2-030. K_2SeO_4. κ'', $\mathrm{Im}(\kappa^{-1})$ vs. ν [85Ech]. T = RT. The curves were obtained from the infrared reflectivity spectra. Solid curves: transverse optical (TO) phonons (κ''). Dotted curves: longitudinal optical (LO) phonons ($\mathrm{Im}(\kappa^{-1})$). Polarization of the infrared radiation and the corresponding phonon symmetries are shown in the figure.

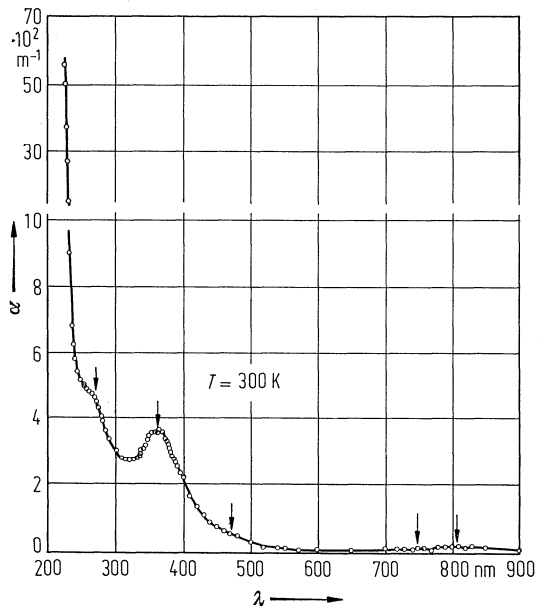

Fig. 39A-2-031. K_2SeO_4. α vs. λ [83Pac]. α: optical absorption coefficient. Arrows indicate absorption bands due to Fe^{3+} impurity centers.

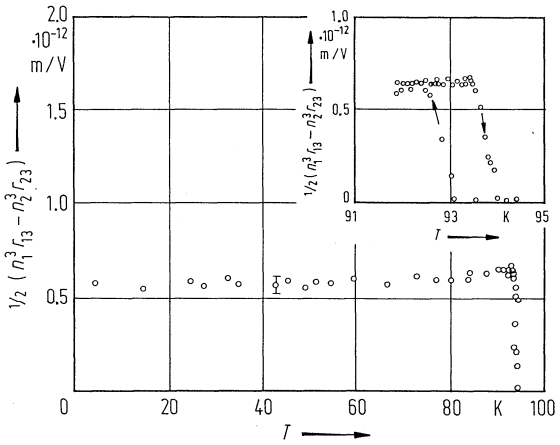

Fig. 39A-2-032. K_2SeO_4. $\frac{1}{2}(n_1^3 r_{13} - n_2^3 r_{23})$ vs. T [82Kro]. $\lambda = 633$ nm.

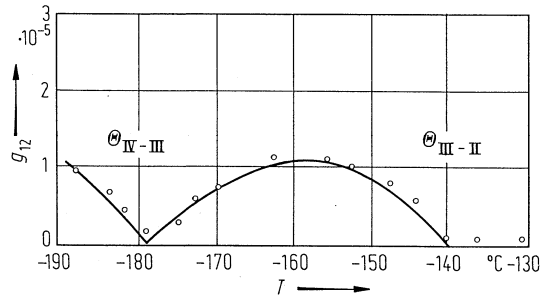

Fig. 39A-2-033. K_2SeO_4. g_{12} vs. T [85Ues]. g_{12}: gyration tensor component. $\lambda = 632.8$ nm.

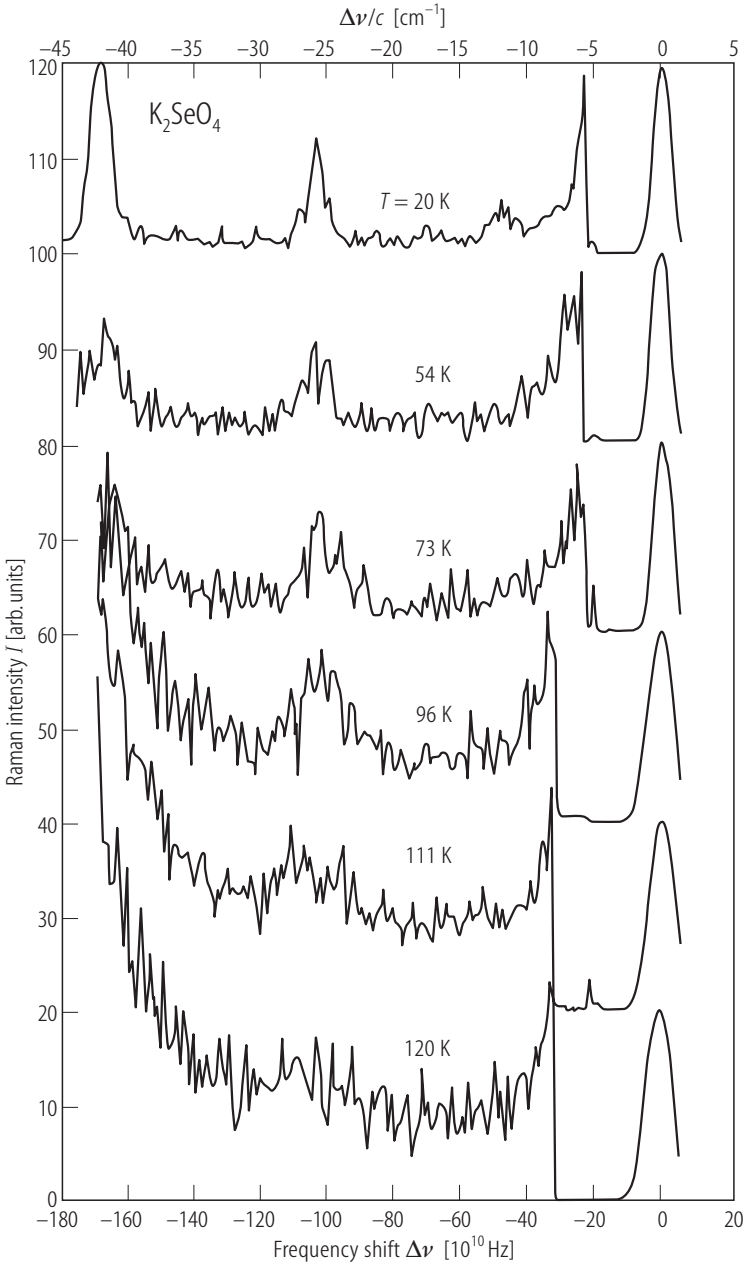

Fig. 39A-2-034. K_2SeO_4. *I* vs. $\Delta\nu$ [89Lee]. Parameter: *T*. *I*: Raman scattering intensity observed in the *c*(*bc*)*b*. $\Delta\nu$: Raman frequency shift.

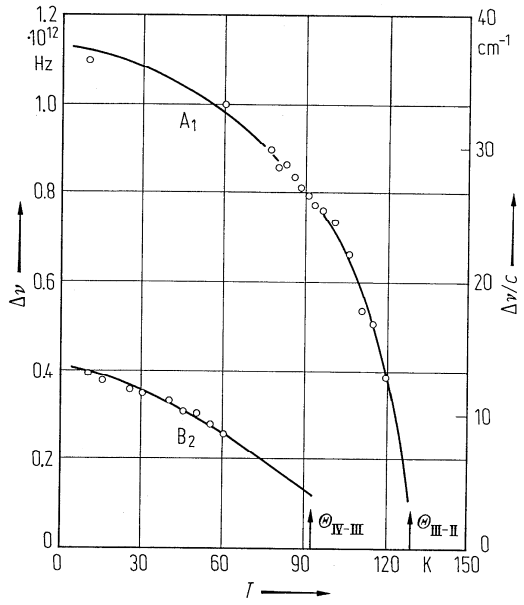

Fig. 39A-2-035. K_2SeO_4. $\Delta\nu$ vs. T [77Wad2]. $\Delta\nu$: Raman frequency shift of the soft A_1 mode and the soft B_2 mode. The data for the A_1 mode are partly provided from [77Wad1].

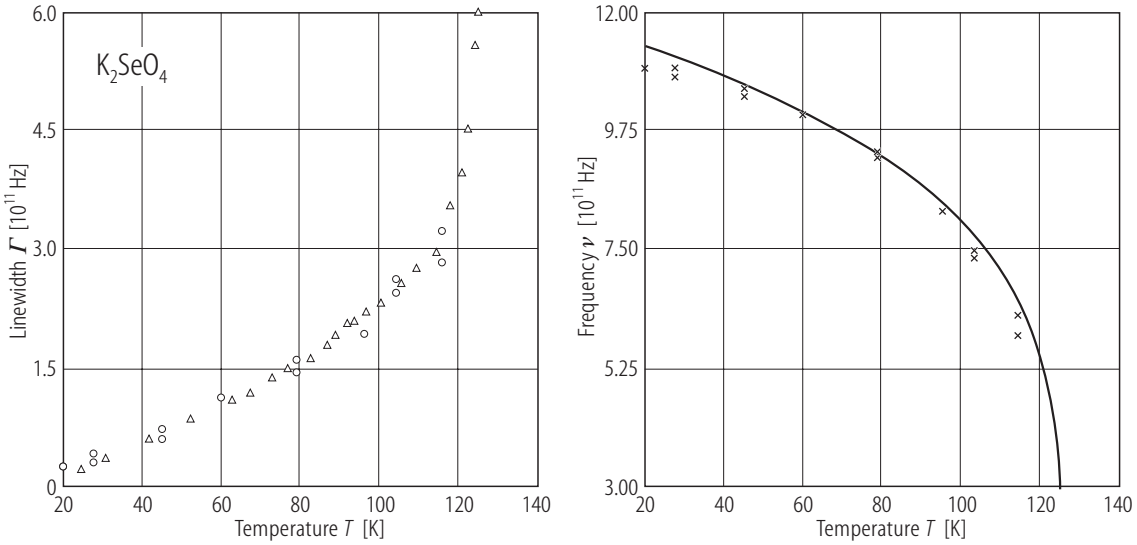

Fig. 39A-2-036. K_2SeO_4. ν, Γ vs. T [88Lee]. Raman scattering. ν, Γ: frequency and linewidth of the amplitude mode. Triangle: linewidth from [79Unr].

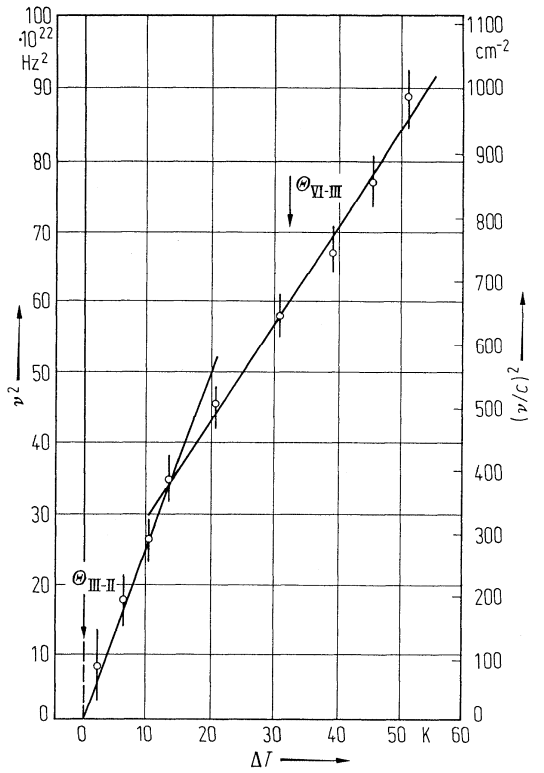

Fig. 39A-2-037. K_2SeO_4. ν^2 vs. ΔT [79Fle]. $\Delta T = T_m - T$. T_m refers to the temperature at which the central peak scattering is maximum, and is approximately equal to Θ_{III-II}. ν: soft mode frequency in $c(a, a)b$ scattering geometry.

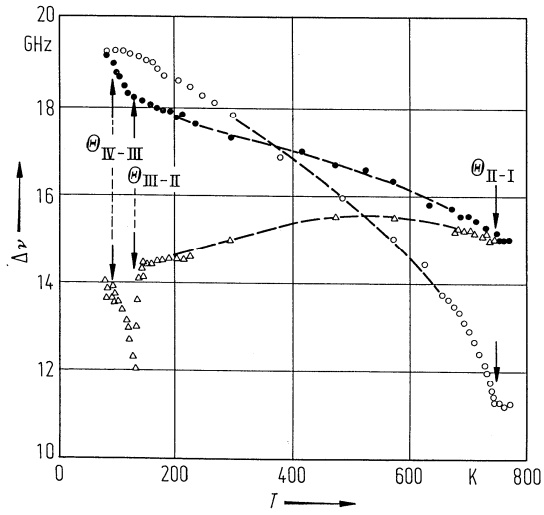

Fig. 39A-2-038. K_2SeO_4. $\Delta\nu$ vs. T [81Yag]. $\Delta\nu$: Brillouin scattering frequency shift. Open circle: $\boldsymbol{q}$ || [100], full circle: $\boldsymbol{q}$ || [010], open triangle: $\boldsymbol{q}$ || [001]. $\lambda = 514.5$ nm.

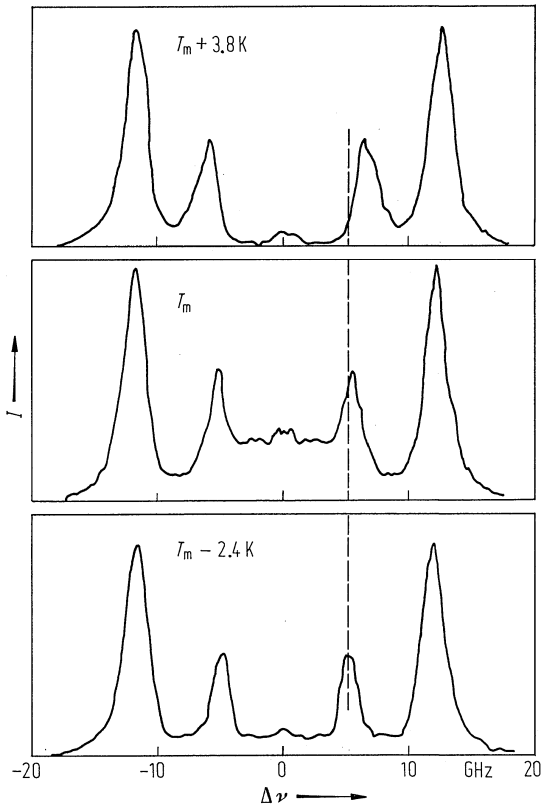

Fig. 39A-2-039. K_2SeO_4. Polarized Brillouin spectra near Θ_{III-II} [79Fle]. Dynamic central peak is observed with the shifting mixed acoustic mode in $c(a, a)b$ scattering geometry. T_m: the temperature at which the central peak scattering is maximum, and is approximately equal to Θ_{III-II}.

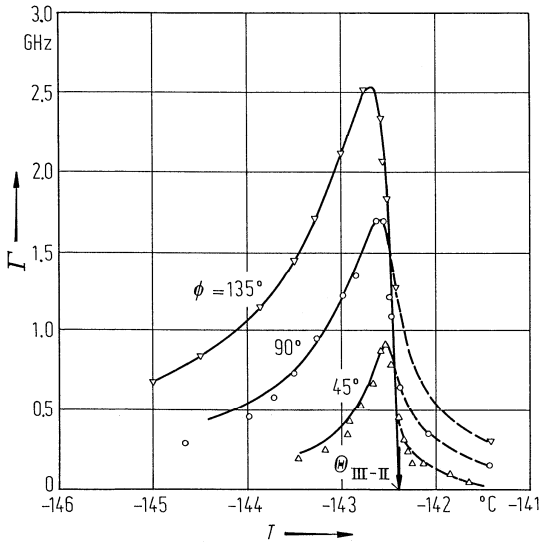

Fig. 39A-2-040. K_2SeO_4. Γ vs. T [84Lus2]. Parameter: scattering angle ϕ. Γ: full linewidth at half maximum of an acoustic phonon spectrum propagating along the c axis. $\lambda = 514.5$ nm.

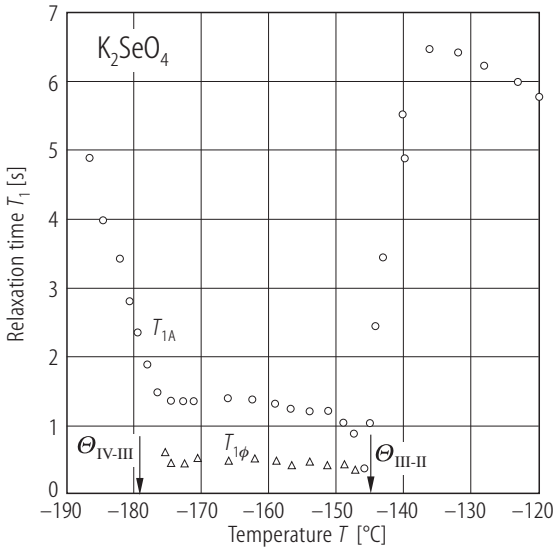

Fig. 39A-2-041. K_2SeO_4. T_1 vs. T [89Top]. T_1: ^{39}K spin-lattice relaxation time. T_{1A}: T_1 measured at the edge singularities, $T_{1\phi}$: at the center of the incommensurate frequency distribution. ν_L = 16.6283 MHz.

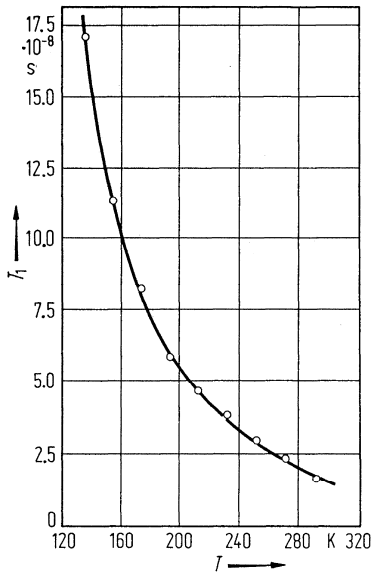

Fig. 39A-2-042. K_2SeO_4. T_1 vs. T [70Aik2]. T_1: spin-lattice relaxation time for $(SeO_4)^-$ produced by ^{60}Co γ-rays.

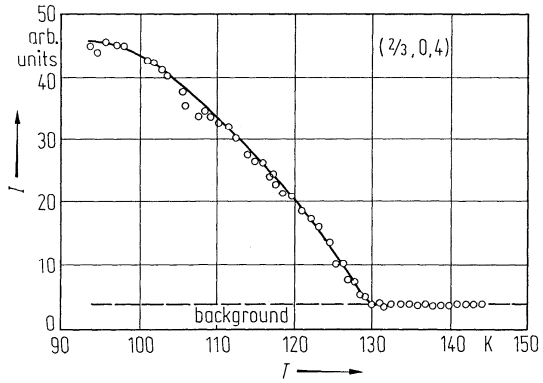

Fig. 39A-2-043. K_2SeO_4. I vs. T [75Ter]. I: peak intensity of X-ray Bragg reflection at (2/3, 0, 4).

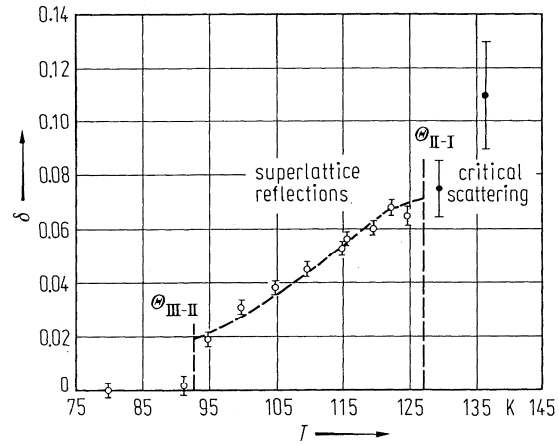

Fig. 39A-2-044. K_2SeO_4. δ vs. T [77Iiz]. δ: misfit parameter which is related to modulation wavenumber vector $\boldsymbol{q}$ as $\boldsymbol{q} = 1/3(1 - \delta)\boldsymbol{a}^*$, $\boldsymbol{a}^*$: reciprocal lattice vector in phase II.

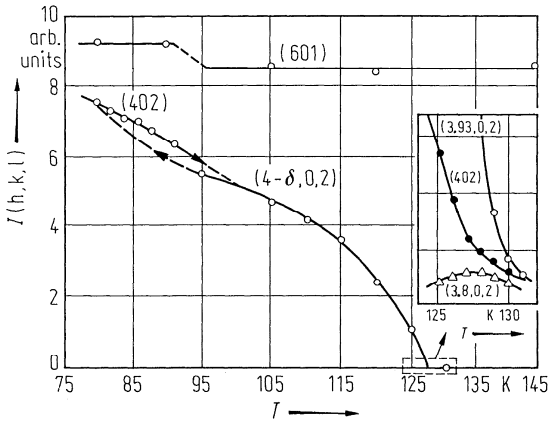

Fig. 39A-2-045. K_2SeO_4. I(h, k, l) vs. T [75Ter]. I(h, k, l): neutron intensities of fundamental reflection at (6, 0, 1) and satellite reflection at (4 – δ, 0, 2). For the meaning of δ, see Fig. 39A-2-044. Insert: intensities at a few fixed points around (4 – δ, 0, 2).

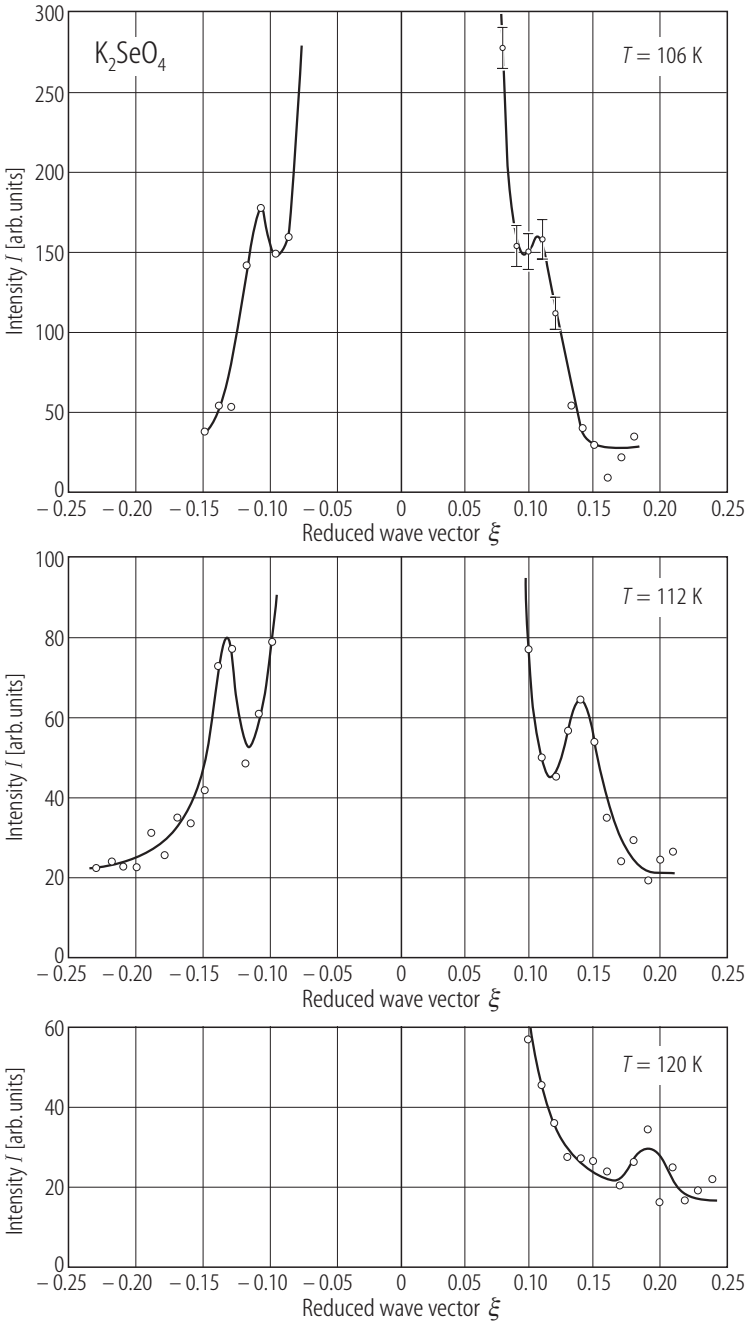

Fig. 39A-2-046. K_2SeO_4. I vs. ξ [77Iiz]. Parameter: T. I: neutron scattering intensity at (6 + ξ, 0, 2). Energy of incident neutron is 14.6 meV.

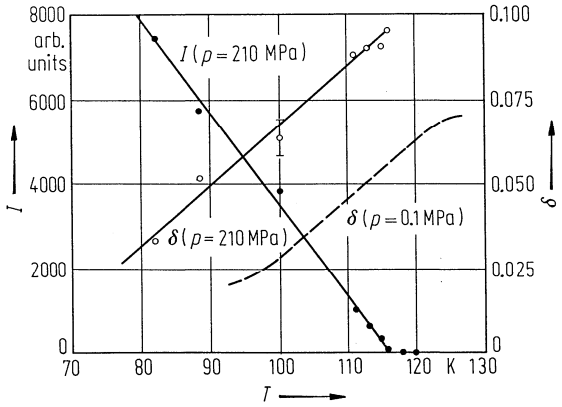

Fig. 39A-2-047. K_2SeO_4. I, δ vs. T [80Pre]. Parameter: p. I: intensity of neutron diffraction peak at (ξ, 0, 2) with $\xi = (4 - \delta)a^*/3$. a^*: reciprocal lattice constant. For the meaning of δ, see Fig. 39A-2-044. The data at atmospheric pressure are provided from [77Iiz].

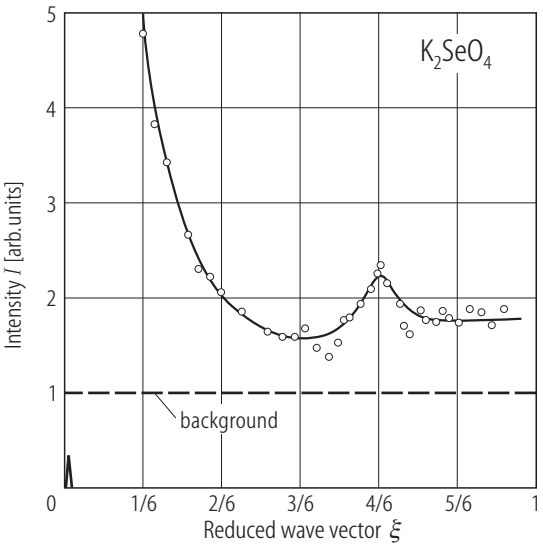

Fig. 39A-2-048. K_2SeO_4. I vs. ξ in phase II [75Ter]. I: X-ray diffuse scattering intensity at (ξ, 0, 4). $T = \Theta_{III-II} + 2$ K. Small triangle in the figure indicates the size of the resolution.

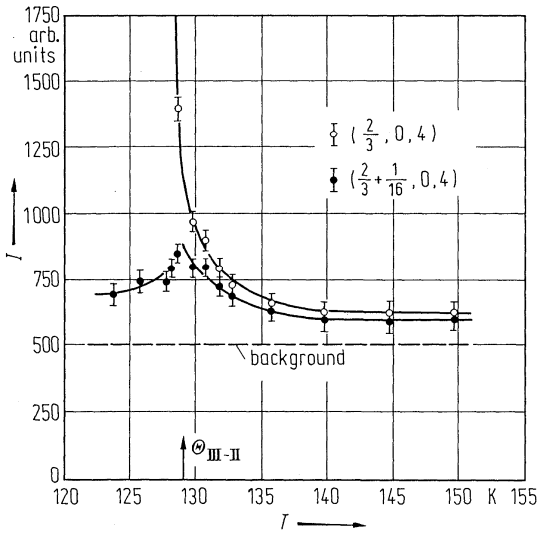

Fig. 39A-2-049. K_2SeO_4. *I* vs. *T* [75Ter]. *I*: X-ray diffuse scattering intensity.

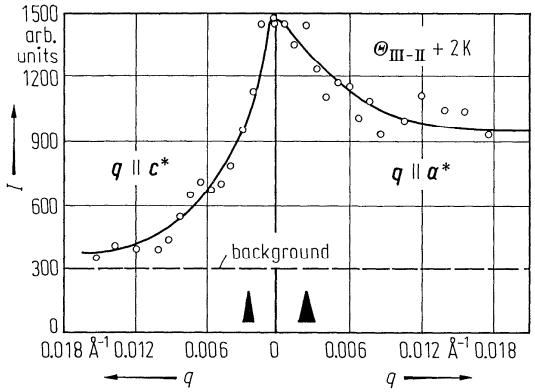

Fig. 39A-2-050. K_2SeO_4. X-ray diffuse scattering around (2/3, 0, 4) in phase II [75Ter]. $T = \Theta_{III-II} + 2$ K. Triangles indicate the size of the resolution in the figure.

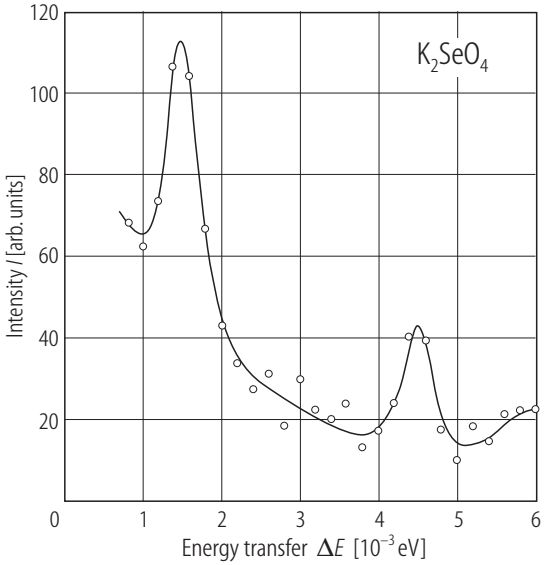

Fig. 39A-2-051. K_2SeO_4. Neutron scattering spectrum at (4/3, 0, 4) [80Axe]. ΔE: energy transfer. T = 20 K.

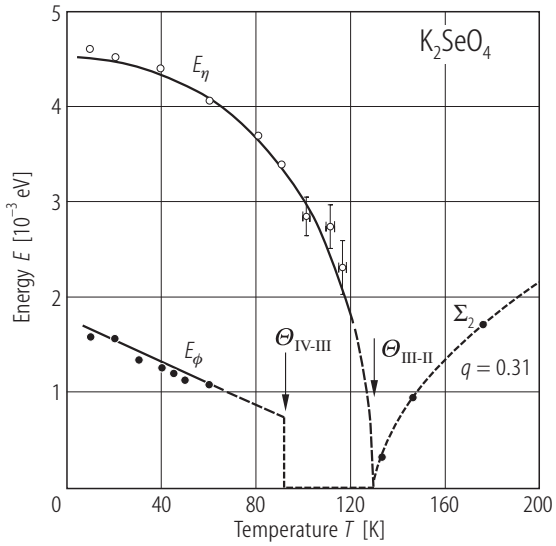

Fig. 39A-2-052. K_2SeO_4. E vs. T [80Axe]. E: energy of q = 0 phase mode (E_ϕ) and amplitude mode (E_η). Solid lines are Raman scattering results [77Wad1, 77Wad2]. Data points are neutron results; results above Θ_{III-II} are provided from [77Iiz].

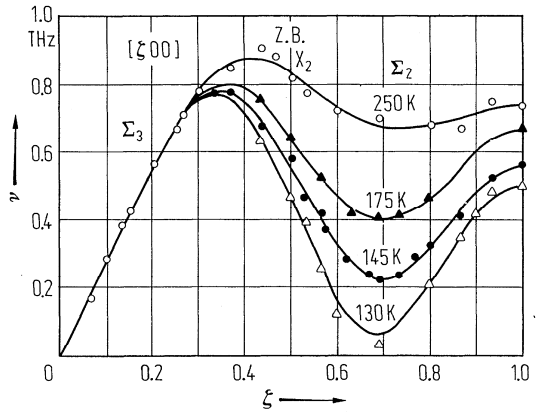

Fig. 39A-2-053. K_2SeO_4. ν vs. ζ in an extended zone [77Iiz]. Parameter: *T*. Z.B: zone boundary.

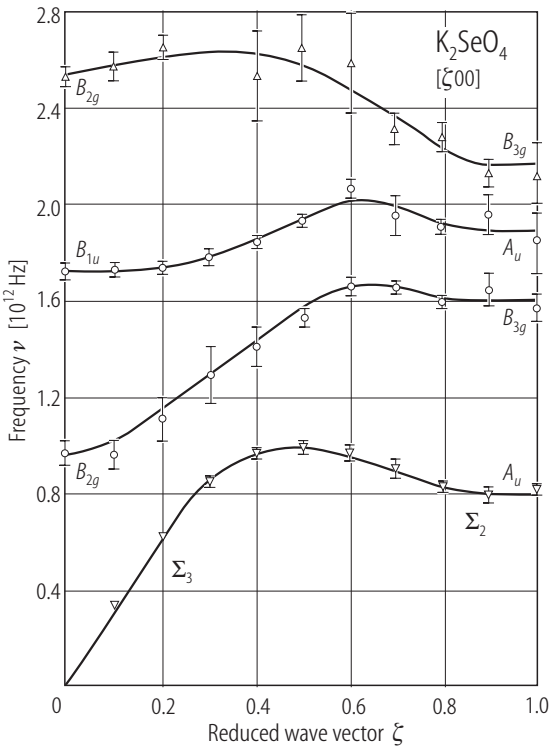

Fig. 39A-2-054. K_2SeO_4. ν vs. ζ in an extended zone [92Etx]. $T = 300$ K.